Soft Matter

PAPER

View Article Online
View Journal

Cite this: DOI: 10.1039/c4sm01071j

High-speed, high-purity separation of gold nanoparticle–DNA origami constructs using centrifugation†

Seung Hyeon Ko,‡[ab] Fernando Vargas-Lara,[c] Paul N. Patrone,[ad] Samuel M. Stavis,[a] Francis W. Starr,[e] Jack F. Douglas[c] and J. Alexander Liddle*[a]

DNA origami is a powerful platform for assembling gold nanoparticle constructs, an important class of nanostructure with numerous applications. Such constructs are assembled by the association of complementary DNA oligomers. These association reactions have yields of <100%, requiring the development of methods to purify the desired product. We study the performance of centrifugation as a separation approach by combining optical and hydrodynamic measurements and computations. We demonstrate that bench-top microcentrifugation is a simple and efficient method of separating the reaction products, readily achieving purities of >90%. The gold nanoparticles play a number of critical roles in our system, functioning not only as integral components of the purified products, but also as hydrodynamic separators and optical indicators of the reaction products during the purification process. We find that separation resolution is ultimately limited by the polydispersity in the mass of the gold nanoparticles and by structural distortions of DNA origami induced by the gold nanoparticles. Our study establishes a methodology for determining the design rules for nanomanufacturing DNA origami–nanoparticle constructs.

Received 16th May 2014
Accepted 15th July 2014

DOI: 10.1039/c4sm01071j

www.rsc.org/softmatter

1. Introduction

Structural DNA nanotechnology has evolved since the early 1980s when Nadrian Seeman first proposed that DNA molecules could be used as nanoscale building blocks.[1] A significant acceleration has occurred recently, following the demonstration of high-yield, discrete, readily-functionalized DNA nanostructures by Rothemund[2] and others.[3–6] The field has now reached a critical juncture, with practical applications becoming a real possibility as techniques for assembling more complex, multifunctional nanostructures are developed. For this potential to be realized, however, a number of nanomanufacturing issues must be addressed, including the relatively high rate of assembly errors, slow assembly process, limited scale, and high cost of starting materials.[7,8] A number of groups have made progress in some of these areas, with improvements in the time taken to assemble complex structures[9] and the development of novel schemes to increase the scale and speed of the production of DNA nanostructure component parts.[10]

Despite these advances, obstacles to widespread deployment of DNA-based assembly processes remain. In particular, one of the most attractive features of structural DNA nanotechnology – its ability to precisely organize disparate nanomaterials into heterogeneous nanostructures – is difficult to take advantage of due to the lack of suitable, scalable purification methods. These methods are essential because the attachment yield of nanocomponents for any target nanostructure is less, often much less, than 100%.[11] The problem of separating the desired product from unreacted or incompletely reacted species, and mis-assembled structures becomes compounded as more species of nanostructure, with potentially different attachment mechanisms, are engineered into these constructs. Practical solutions to such multidisciplinary problems lie at the intersection of biology, chemistry, physics and engineering, motivating a systems-level approach – combining theory and experiment – to designing and fabricating structures with the desired functionality at high yields and purities.

In contrast, the most commonly used method for separating well-folded DNA nanostructures from other by-products, agarose gel electrophoresis, has not been optimized at the

[a]Center for Nanoscale Science and Technology, National Institute of Standards and Technology, Gaithersburg, MD 20899, USA. E-mail: liddle@nist.gov
[b]Maryland Nanocenter, University of Maryland, College Park, MD 20742, USA
[c]Material Science and Engineering Division, National Institute of Standards and Technology, Gaithersburg, Maryland 20899, USA
[d]Department of Physics, Institute for Research in Electronics and Applied Physics, and Condensed Matter Theory Center, University of Maryland, College Park, Maryland 20742-4111, USA
[e]Department of Physics, Wesleyan University, Middletown, Connecticut 06457, USA

† Electronic supplementary information (ESI) available. See DOI: 10.1039/c4sm01071j

‡ Current address: Center for Nanomaterials and Chemical Reactions, Institute for Basic Science (IBS), Daejeon 305-701, Korea.

system level, and suffers from severe technical limitations in the present context.[12] First, only a small ($\approx$10 μL, $\approx$1 picomole) quantity of sample can be loaded onto a gel. Then, there is a need for a reference material against which to calibrate the electrophoretic mobility of the products. Further, in separations of nanohybrid structures, such as AuNPs attached to DNA origami, the electrophoretic mobility of the construct is essentially the same as that of the origami, leading to a lack of resolution in the gel that makes effective separations all but impossible (Fig. S1†).[13,14] Following separation, recovery yields of the products after extraction from the gel pieces when using electroelution or a freeze-squeeze column are less than 100%, and the desired structures may also be damaged. Finally, it may be difficult to remove residual gel from the products.

These limitations have led to the search for alternative separation/purification methods. Centrifugation in various forms[15] has a long history in the preparation and analysis of large biomolecules[16] and can achieve very high separation resolution.[17] Shih and co-workers recently reported the use of ultracentrifugation (using accelerations of up to 300 000 × g) in a glycerol gradient to separate well-formed DNA origami structures from excess staple strands and origami multimers.[18] Centrifugation separation has also been actively used for sorting nanostructures including nanoparticles[19–23] and carbon nanotubes (CNTs). In the latter case, the precise separation of CNTs according to their electrical and structural properties has been shown.[24–27] However, until now, the effectiveness of rate-zonal centrifugation for the separation of more complex constructs involving heterogeneous nanomaterials has not been demonstrated.

Here, we show that rate-zonal centrifugation in a basic, bench-top microcentrifuge is a simple method for separating DNA origami–AuNP constructs from unwanted nanostructures and reactants, and that it further allows the extraction of specific, and even multiple, target products with high efficiency. In our design for nanomanufacturing approach, we use gold nanoparticles, arguably one of the most important constituents of many DNA-based heterostructures,[28–37] as a multifunctional component that: confers useful optical properties, serves as a means of separating out the target constructs, and also acts as a visual marker enabling facile extraction of the desired product. Simultaneously, we choose the configuration of the AuNP binding sites to maximize binding yield, and the centrifugation medium to simplify product extraction and purification. In this way, we demonstrate that rate-zonal centrifugation, at modest accelerations in a bench-top microcentrifuge, is an efficient, scalable separation technique, with high recovery yields that delivers purities of >90%.

Rate-zonal centrifugation separation is performed by loading the sample solution in a narrow ($\approx$0.5 mm) single layer on top of a gradient medium inside a 2.0 mL microcentrifuge tube. The tube is centrifuged under a combination of acceleration and gradient medium density and viscosity, chosen in this case, to achieve separation in a few hours in a bench-top microcentrifuge. The objects sediment through the medium under the collective influence of three forces: centrifugal force (F_C), ($\propto$mass), buoyant force (F_B), ($\propto$volume), and drag force (F_D), ($\propto$hydrodynamic radius). Ideally, the resultant of these three forces should be sufficiently different for different objects to yield distinct (*i.e.*, maxima more than one standard deviation apart) bands that can then be extracted from the tube. We note that the large density of the origami–AuNP constructs precludes the use of isopycnic centrifugation. That method relies on the construction of a density gradient through which objects sediment until they reach a position where the density of the surrounding medium is the same as that of the object itself. Isopycnic centrifugation has been commonly used for separating biomolecules and, more recently, carbon-based nanomaterials, but any cluster or rational assembly of more dense nanoparticles (*e.g.*, gold) cannot be sorted using this technique due to the lack of separation media with sufficiently high density. While the use of high-density AuNPs precludes isopycnic separation, it does make it possible to engineer the mass of the desired product thereby enabling efficient separations to be performed.

In this work, we investigate rate-zonal centrifugation in an iodixanol gradient as a means to separate a variety of AuNP–DNA constructs and examine the effect of AuNP size, number, and the complex interactions between nanoparticles and origami on the performance of this approach. The ability to resolve different constructs depends on the details of the hydrodynamic behaviour and mass of the constructs. We also find that the DNA origami–AuNP system exhibits conformational changes due to Au–DNA interactions, with important implications not only for the performance of this separation and purification method, but also for the design, synthesis and application of such constructs. We employ dynamic light scattering (DLS) to measure the hydrodynamic size, R_H, of the various constructs and use simulations to explain the observed non-monotonic variation in R_H, with increasing AuNP size and number.

2. Results and discussion

2.1 Separation of DNA origami–AuNP complexes

We fabricated nAuNP–DNA origami (n =1, 2, and 3; the number of AuNP bound onto DNA origami) using rectangular DNA origami (70 nm × 100 nm) as a template. Each binding location for AuNPs consists of three hybridizing staple strands, modified by extending them with 22 adenines (A) at pre-defined positions. AuNPs were fully covered with single strands of 18 thymines (T) (di-thiolated at the 5′-end), in order to avoid aggregation of AuNPs at the high concentration of Mg^{2+} needed to stabilize the origami. We constructed three different patterns (n = 1, 2, and 3) of AuNPs on DNA origami by mixing AuNP solution with the origami template solution at a stoichiometry of 2 : 1 (AuNP–binding site), and cooling overnight from 37 °C to room temperature. We purified these samples directly by centrifugation separation without any pre-treatment.

We performed rate-zonal centrifugation of nAuNP–origami using a nine-layer density/viscosity gradient (made with 10%, 15%, …, 50% mass concentration of iodixanol in tris(hydroxymethyl) aminomethane-acetate-(ethylenediamine tetraacetic acid) (1× TAE/Mg^{2+}), Table S1†) and centrifugation in a bench-top microcentrifuge at an acceleration chosen to separate

constructs with a given AuNP size within a period of <270 min. We used a swing-bucket rotor for centrifugation. In this configuration, the centrifuge tubes swing out to a horizontal position during rotation, thus maximizing the distance the materials travel through the separation medium and eliminating the band distortion that can occur in fixed-rotor systems in which the separation medium slides down the wall of the centrifuge tube. As a gradient material, we chose iodixanol (density = 1.32 g cm^{-3} and dynamic viscosity = 14.3 mPa s for a 60% volume fraction of iodixanol in water, Table S1† and Fig. S2†) which is non-ionic and has good solubility in water. This material also exhibits minimal hydrogen bonding interactions, and can therefore be readily separated from DNA, unlike glycerol. We also note that it is *necessary* to use a gradient medium to avoid convection currents which tend to destroy stability of the bands (control experiments are shown in Fig. S3†).[38,39]

To demonstrate the separation efficacy of centrifugation, we tested various AuNP–DNA origami constructs using AuNPs with nominal diameters of 5 nm, 10 nm, 15 nm, 20 nm, and 30 nm with actual core-size distributions of the AuNPs measured by transmission electron microscopy (TEM). Fig. 1 shows the evolution of the sedimentation distribution for 10 nm *n*AuNP–DNA origami constructs (n = 1, 2, and 3). The plasmon absorption of the AuNPs functions as a visual indicator of the separation process, obviating the need for fraction-by-fraction analysis of the tube contents to determine construct location.[18]

We monitored band separation by using the intensity of the absorption as a function of position along the centrifuge tubes at different time intervals. After 270 minutes of centrifugation at 850 rad s^{-1} (68 600 m^2 s^{-1}, 7000 × g), several distinct red bands were clearly visible in the centrifugation tubes as shown in Fig. 2a. We investigated the performance of the separation by recovering each band from the medium by pipetting, followed by buffer exchange using centrifuge filtration, followed by

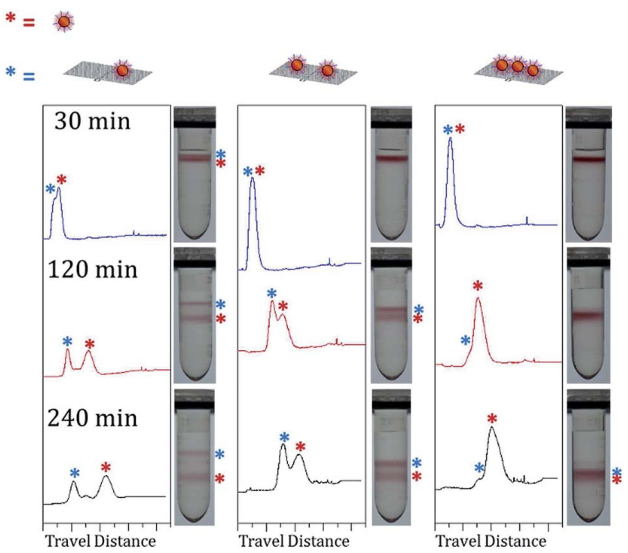

Fig. 1 Evolution of sedimentation distribution of various constructs of *n*10 nm AuNP–DNA origami at different time intervals as indicated by digital photographs of centrifuge tubes and corresponding optical density measurements.

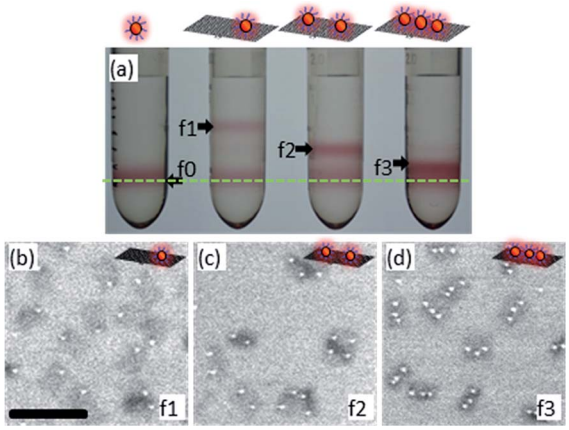

Fig. 2 Separation of *n*10 nm AuNP–DNA origami. (a) Photograph of centrifuge tubes containing different constructs after spinning for 270 min. at 850 rad s^{-1} (8100 rpm, 68 600 m s^{-2}, 7000 × g). (b)–(d) Typical SEM images of different fractions of AuNP–origami constructs as labelled in (a). Schematics of the target product are shown for each tube. The fraction labelled f0 corresponds to free AuNPs. The SEM scale bar is 200 nm.

inspection of the constructs by scanning electron microscopy (SEM) (Fig. 2b–d). Analysis of the SEM images reveals purities of better than 90% for each fraction: f1 is (96.1 ± 0.5)% 1AuNP–origami, f2 is (94.6 ± 1.0)% 2AuNP–origami, and f3 is (92.9 ± 1.3)% 3AuNP–origami. Unless otherwise noted all measurements are reported as (average ± one standard deviation). Additional SEM images of larger areas for each fraction are provided in the supporting information (Fig. S4a–c†). In addition to the high purity of each fraction, the process is highly efficient (Fig. S5†), with the amount of material recovered close to the starting amount – suitable for immediate application or enabling further fabrication steps.

As shown in Fig. 2a, the band corresponding to 3AuNP–origami fraction, f3, is adjacent to that of the fraction f0, corresponding to free AuNPs, making separation difficult in this case. It is therefore important to understand the degree to which constructs can be engineered to enable the separation of different constructs from one another and from the starting materials.

During centrifugation, objects with the same sedimentation coefficient, s, travel through the medium as a narrow band: s depends on the mass, volume and hydrodynamic size of the constructs according to the Svedberg equation,

$$s = \frac{\mathrm{d}r/\mathrm{d}t}{\omega^2 r} = \frac{m - V\rho_s}{6\pi\eta_s R_H} \quad (1)$$

where ω is the angular velocity, r is the distance of the object from the rotation axis, m is the mass of the object, R_H is the hydrodynamic radius of the object, V is volume of the object, η_s is the dynamic viscosity of the fluid, and ρ_s is the density of the fluid. Eqn (1) is derived in the ESI.† In the case of a density gradient medium, both ρ_s and η_s are functions of r. R_H may also vary with r, depending on the interaction of the DNA with the gradient medium. We neglect this latter effect in our analysis because we expect it to influence only the apparent thickness of

the shell of single-stranded DNA (ssDNA) on the AuNPs, but not the origami, which is a much more constrained structure. As expected, the sedimentation velocity of 10 nm *n*AuNP–DNA origami constructs increases with *n*, while the band of free AuNPs – having the largest m/R_H ratio – sediments most rapidly through the medium. The hydrodynamic size of the AuNPs increases dramatically upon binding to the free origami, which has an R_H of (35.0 ± 1.4) nm. This more than compensates for the mass added by the origami.

We estimate our ability to resolve the different species into separate bands using the sedimentation coefficients calculated for each construct from eqn (1) to estimate the distance travelled during centrifugation. As a starting point for this calculation, we assume that the hydrodynamic radius of constructs containing *n*AuNPs is constant, dominated by the size of the DNA origami, and is unaffected by the number of attached AuNPs. We expect this naïve assumption to be reasonably good for particles that are small relative to the origami, but to break down at larger particle sizes. We calculate the mass of the constructs using the known densities of DNA and Au and the designed and measured sizes of the DNA and Au components, respectively. We compare our estimates to data obtained from "centrifugrams" – measurements of optical density taken from digital photographs – as a function of *r* (Fig. S6†). Analysis of the resulting curves allows us to measure the centre and width of each band and hence determine the average and standard deviation of the normalized travel distance of each construct. We note that the full-width at half-maximum (FWHM) of the observed bands is controlled by that of the AuNP size, and hence mass, distributions – both the initial width of the solution (≈0.5 mm) upon loading in the centrifuge tube and diffusion occurring during centrifugation are minor contributors.[40]

Fig. 3 shows the results of calculations of the sedimentation coefficients for free gold nanoparticles and 1AuNP–origami constructs *vs.* nominal particle size for a flat viscosity profile and infinite tube length (Plots for Ag and CdSe nanoparticles are included in the ESI (Fig. S18†) for comparison). A plot for our actual experimental conditions is shown in the ESI (Fig. S19†). Although the absolute band positions change with the details of the viscosity profile, the relative positions are unchanged. Separation of constructs with purities >90% is not possible for nominal particle diameters smaller than 6 nm or larger than 27 nm because the change in sedimentation coefficient caused by the addition of the particle to the origami for small particles, or the origami to the particle for large particles, is less than the variation in sedimentation coefficient (which corresponds to band width) due to particle polydispersity.[41]

Fig. 4 shows a plot of the normalized calculated and experimental centrifugram peak locations and widths for each set of constructs containing 10 nm, 15 nm, 20 nm and 30 nm AuNPs (Fig. S7–S16†). By estimating the area under each peak and taking account of the total number of AuNPs present, we are able to obtain a qualitative indication of the yield of each fraction in cases where a mixture of products is generated. This yield estimation method is a useful diagnostic tool for optimizing assembly conditions. A comparison of the measured *vs.* calculated sedimentation distances indicates that, although the calculations capture the overall trends reasonably well, there are significant discrepancies with the experimental data. In particular, while the experimental normalized travel distances

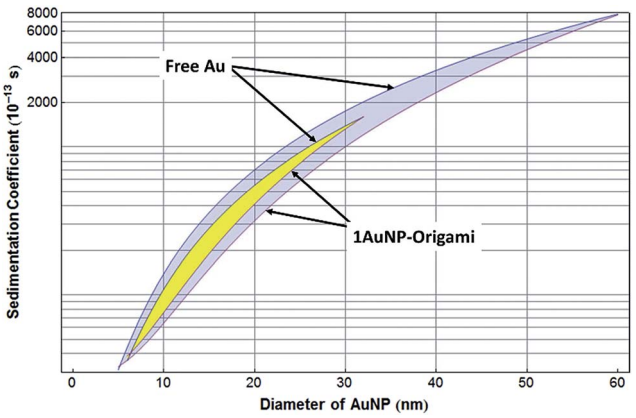

Fig. 3 Sedimentation coefficient *versus* particle size for free gold nanoparticles and 1AuNP–origami constructs. The large shaded area represents the range of particle sizes over which separations between free AuNPs and AuNP–origami constructs can be achieved, assuming a monodisperse size distribution. The small shaded area represents the range of particle sizes over which separations can be achieved, assuming a size distribution which varies between ±10% about the average.

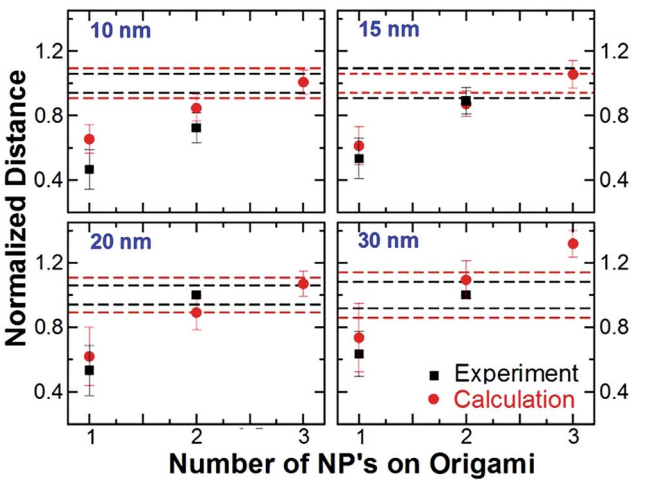

Fig. 4 Band displacement distances following centrifugation of *n*AuNP–DNA origami normalized against those of the corresponding free AuNP. The dashed lines correspond to the normalized free AuNP travel distance variations (red circles – calculated, black squares – measured). The experimental distances were determined from the peaks in optical density measurements of digital photographs of the centrifuge tubes. The experimental error bars correspond to the standard deviations of the peaks (derived from the FWHM, assuming an approximately Gaussian distribution). The calculated bars are determined by using the experimentally determined standard deviations of the particle size distributions derived using Gaussian fits to the TEM data (extensive measurements of similar AuNPs show quite complex distributions) to estimate the range in travel distances for Au NPs of different sizes. The bars are normalized to the travel distances of their respective peaks.

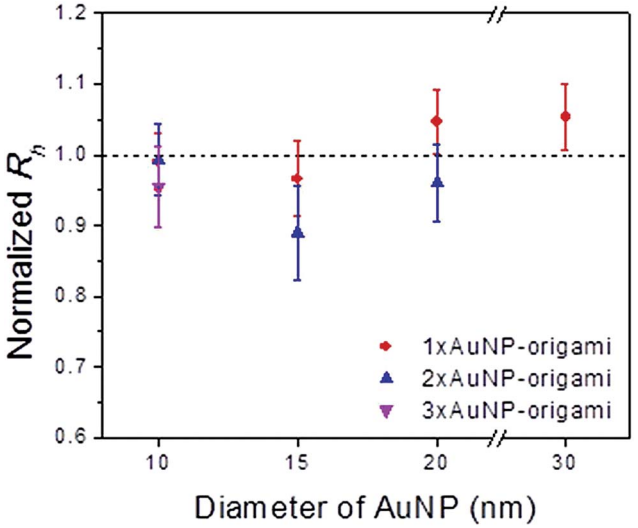

Fig. 5 Hydrodynamic radii of AuNP–origami constructs in buffer measured by dynamic light scattering. Hydrodynamic radii of the constructs are normalized by the radius of free origami ((35.0 ± 1.4) nm). The bars represent one standard deviation for variation of different batches (measurements taken from at least three different samples prepared on three different days).

generally lie below the estimated ones, those measured for both the 15 nm and 20 nm 2AuNP–origami do not follow this trend. Since the mass of each construct is well defined within the limits discussed above, variations in the hydrodynamic radius are the most likely cause of changes in the sedimentation behaviour. In order to investigate this effect further, we compared the measured and simulated hydrodynamic radii of AuNPs, before and after DNA attachment, and of the various *n*AuNP–origami constructs (Fig. 5).

2.2 Simulation of R_H of origami, ssDNA–AuNPs and AuNP–origami complexes

It is apparent from Fig. 5 that the AuNPs have a significant influence on the hydrodynamic radius of the constructs. Rather than simply remaining constant or increasing with the addition of more or larger AuNPs, we observe a non-monotonic variation in R_H as more AuNPs are added. This effect is pronounced for the 15 nm and 20 nm 2AuNP–origami constructs – consistent with our observations from Fig. 4. To explore this counter-intuitive phenomenon, we first use molecular dynamic simulations of coarse-grained models of DNA-functionalized Au nanoparticles, origami, and *n*AuNP–origami complexes to determine their respective structures. We then apply the ZENO program[42–44] for computing the hydrodynamic radii of complex-shaped particles to calculate the hydrodynamic radii of each species. ZENO is capable of computing the R_H of objects of complex and essentially arbitrary initial specified geometry, a task not possible by analytic computation, and currently infeasible by molecular dynamics simulations for particles having the size and intricate shape of the AuNP–origami complexes (even the R_H of an individual flexible chain cannot currently be accurately calculated analytically).[42,43,45]

The structure of the origami, DNA-functionalized Au nanoparticles and *n*AuNP–origami complexes is determined using a coarse-grained model reported previously.[46,47] We represent DNA strands as a chain of "beads", connected by non-linear springs. In the following figures, the ssDNA attached to the AuNP is shown as blue spheres, the double-stranded DNA (dsDNA) in the origami is shown as grey spheres, and the AuNP cores are depicted as red spheres. The AuNP model used here is a small modification of the one introduced in ref. 42–44, and the origami molecular model corresponds to a modified version of that presented in ref. 46.

We treat the ssDNA as a chain with a distance between bases of ≈0.65 nm and employ a Kremer–Grest (KG) potential[48] to model the interaction between bases. This potential is described by the sum of a Weeks–Chandler–Andersen (WCA) potential (U_{WCA}) accounting for non-bonded, inter-molecular excluded-volume interactions and short-range repulsion (eqn(2)), and a finitely extensible non-linear elastic (U_{FENE}) potential to capture intra-molecular interactions (eqn (3)). A three-body angular potential (eqn (4)) accounts for the chain stiffness and determines the persistence length (≈2 nm for ssDNA at the salt concentration used here).[49]

$$U_{WCA}(r) = \begin{cases} 4\varepsilon\left(\left(\frac{\sigma}{r}\right)^{12} - \left(\frac{\sigma}{r}\right)^{6}\right) + \varepsilon, & r < 2^{\frac{1}{6}}\sigma \\ 0, & r > 2^{\frac{1}{6}}\sigma \end{cases} \quad (2)$$

$$U_{FENE}(r) = -\frac{1}{2}k_{FENE}\left(\frac{3}{2}\sigma\right)^2 \log\left[1 - \left(r \Big/ \left(\frac{3}{2}\sigma\right)\right)^2\right] \quad (3)$$

$$U_{linear}(\theta) = k_{linear}[1 + \cos(\theta)] \quad (4)$$

The parameter ε defines the energy scale and is taken to be approximately 2.5 kJ mol^{-1} (equivalent to k_BT), while σ determines the length scale (bead size) and is taken to be ≈0.65 nm –

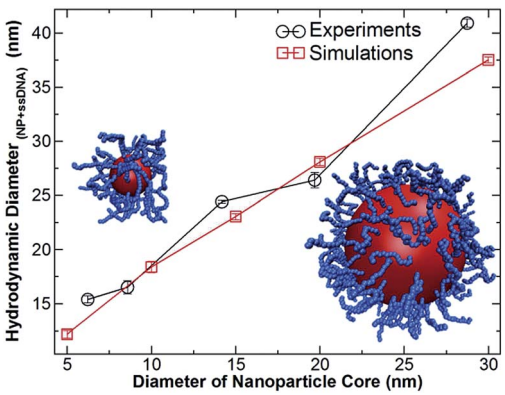

Fig. 6 Comparison of measured and simulated hydrodynamic radii for ssDNA-functionalized AuNPs of nominal radii 5 nm, 10 nm, 15 nm, 20 nm and 30 nm. The experimental vertical bars represent the standard deviation of 3 separate DLS measurements and the vertical bars in simulation data represent the standard deviation obtained from the distribution of the 10^3 simulations performed for each particle type.

the effective length of a single nucleotide in fully extended ssDNA. k_{FENE} is 30ε and k_{linear} is 6ε, to match the persistence length, $L_P = k_{linear}\sigma/2k_BT \approx 2$ nm, of ssDNA.[50]

The AuNPs are also modeled using a WCA potential, but with the origin shifted to move the repulsive interaction to the AuNP particle surface. The AuNPs are functionalized with a number of ssDNA strands that depends on both the AuNP size and the salt concentration used during the attachment process.[51–53] We then perform molecular dynamics simulations for 10^8 time steps to equilibrate the system and apply the ZENO program to compute the R_H for a set of 10^3 configurations for each system: DNA-grafted AuNPs, origami, and *n*AuNP–origami complexes. R_H is determined as the peak value in the probability density function obtained from the 10^3 configurations. The R_H values computed for the functionalized AuNPs are shown in Fig. 6 and are in reasonably good agreement with our measured values of R_H, supporting the model and our choice of input model parameters such as DNA grafting density and DNA molecular dimensions.

At the Mg^{2+} concentrations needed to stabilize the origami, citrate-stabilized Au nanoparticles are not stable against aggregation.[54] However, a high coverage of poly-T results in steric interactions sufficient to prevent salt-induced aggregation.[55] As noted above, the density of ssDNA on the surface of the AuNPs decreases with increasing particle radius, meaning that the particles become, in principle, less stable against aggregation as they become larger – consistent with our and other[56,57] observations that preparing stable suspensions of ssDNA-functionalized AuNPs is more challenging for larger nanoparticles. We also expect that the attractive interaction between the DNA and the AuNP surface becomes stronger with increasing NP size,[58] and can result in binding[59] and attractive interactions with dsDNA.[60] These latter two facts motivate the inclusion of an attractive interaction between the AuNP surface and the dsDNA of the origami in the potentials.

We model the origami ($\approx$100 nm $\times$ 70 nm $\times$ 2 nm) used in these experiments as a rectangle of 154 $\times$ 108 spheres in the x and y directions respectively, connected *via* the FENE potential. Since the origami is not elastically isotropic, we use different spring constants in the two directions ($k_x = 90\varepsilon$ and $k_y = 3\varepsilon$, respectively). The net result is a persistence length, $l_{p\text{-}dsDNA}$ of approximately 59 nm along x (corresponding to that of dsDNA) and a stiffness ratio of 15 between the x and y directions. Our estimate of the stiffness ratio is intended to account for the distance between and flexibility of the crossovers between the dsDNA strands. In order to account for the shear stiffness of the origami, we introduce a potential, U_{perp}, (eqn (5)) that depends on the angle formed by three neighboring beads; two beads that belong to one chain, and one bead from the adjacent chain. In addition, we introduce a weak attractive interaction between the origami and the AuNP using a Lennard-Jones potential (Eq. 6) truncated at $r = 2.5\sigma$ and model two cases, with characteristic energies of 0 and ε, respectively, representing the likely range of interaction strengths. Finally, we mimic the attachment of the DNA-functionalized AuNP to the origami by introducing a harmonic potential (eqn (7)) between the last bead of the ssDNA chains on the NP and the beads on the origami.

$$U_{perp}(\alpha) = \frac{k_{perp}}{2}\left(\alpha - \frac{\pi}{2}\right)^2 \quad (5)$$

$$U_{LJ}(r) = 4\varepsilon\left[\left(\frac{\sigma}{r}\right)^{12} - \left(\frac{\sigma}{r}\right)^{6}\right] \quad (6)$$

$$U_{harm}(r) = \frac{k_{harm}}{2}(r - r_0)^2 \quad (7)$$

The interaction between DNA and the DNA-grafted AuNPs in solution is a complex problem involving a number of competing interactions, which depend on solution conditions – such as pH and salt concentration – DNA sequence, DNA chain mass, the form of the hybridized DNA, and AuNP size. Apart from the naturally attractive interactions between the hybridizing complementary strands of the DNA chains grafted onto the AuNPs and those extending from the origami, we note that DNA molecules themselves can have appreciable, attractive, non-specific interactions with Au and many other interfaces. In particular, ssDNA has been found to bind strongly to macroscopic planar Au interfaces:[61] an effect attributed by Herne and Tarlov to the strong interaction between the (polarizable N) atoms of the DNA nucleotides with the AuNP. On the other hand, Murphy *et al.*[62,63] have found that oligomeric ssDNA *does not* adsorb onto small AuNPs (14 nm) within the range of our measurements. The size of the AuNP thus influences the strength of the binding interaction of the ssDNA with the AuNP. This effect has recently been studied both experimentally[64] and computationally[65] in the context of the adsorption of proteins on small AuNPs. In particular, the simulations of Feng *et al.*[65] emphasize the predominant role of the interaction of polarizable protein atoms (N, O, C) with the Au in understanding this fundamental NP size effect on molecular binding. Such interactions can also be expected to be prevalent in DNA through the presence of the polarizable N atoms in the nucleotides, consistent with the suggestion of the important role of this non-specific interaction between N and Au by Herne and Tarlov. Murphy and coworkers[62,63,66] emphasize that the binding of ssDNA to Au is sequence dependent because of the influence of DNA sequence on the 'coiled' nature of DNA. Any factor influencing the persistence length, or equivalently chain rigidity, of the DNA can be expected to be important in relation to the molecular binding of DNA to Au, since the chain rigidity affects the entropy of association. This effect is clearly evidenced by the fact that oligomeric DNA in its much more rigid duplex form (the persistence length of dsDNA is more than an order of magnitude larger than that of ssDNA)[67] will adsorb strongly onto small Au NPs (14 nm) when single stranded DNA of a given sequence length will not. As with many polymers having a weakly attractive interaction with a substrate, ssDNA will undergo a transition from a non-adsorbed to an adsorbed state on Au with increasing chain length.[62] Importantly, DNA origami is a "woven" form of duplex DNA[2] so that the binding energy of AuNPs to DNA origami can be expected to be *greater* than that of the oligomeric ssDNA grafted onto the AuNP surface. Based on these trends in both experimental and computational studies of

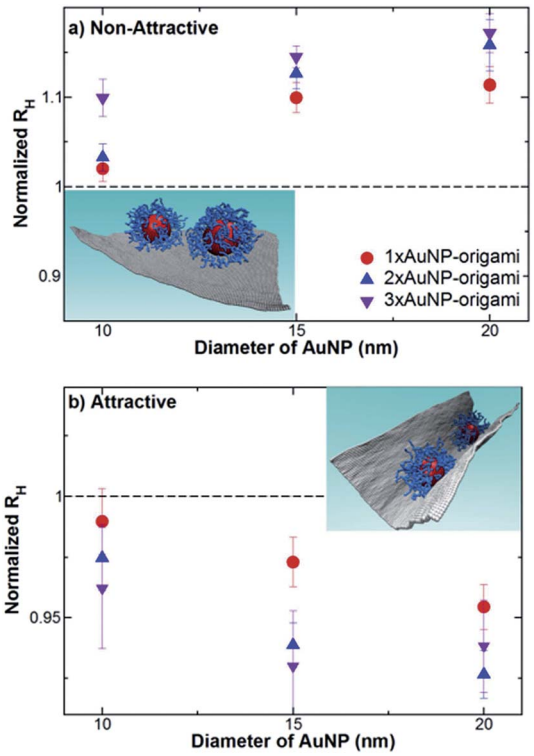

Fig. 7 Simulation of the normalized hydrodynamic radii of *n*AuNP–origami constructs assuming (a) no interaction between the AuNP surface and the dsDNA of the origami, and (b) the result of adding a WCA potential with energy scale ε. Insets show how the conformation of the origami is affected by the interaction with the AuNPs. Vertical bars are one standard deviation.

oligomeric DNA interacting with gold surfaces and AuNPs, we anticipate that the interactions between our AuNPs and the DNA origami will be attractive and strong and will influence the R_H of AuNP–origami constructs and we thus consider the effect of such an interaction in our modeling. Fig. 7a and b show our predicted R_H results for these origami–NP complexes in the extreme cases of a null and attractive interaction, of order kT, between the AuNPs and origami, respectively. When there is no interaction, the origami remains relatively planar, and the R_H increases as more and larger particles are added. When an interaction is present, the overall trends of the experimental data are reproduced, with the same counter-intuitive decrease in R_H as more and larger AuNPs are attached. The particular values of R_H are sensitive to the exact strength of the attractive interaction in the simulation. The influence of the interaction strength on the origami deformation is a topic of ongoing investigation.

These results suggest that the DNA origami cannot be treated as an essentially planar platform, undergoing only modest conformational fluctuations that can accommodate NPs subject to purely geometrical constraints. The excluded volume interactions between the ssDNA on the AuNPs and the dsDNA of the origami and the interactions of the dsDNA of the origami with the AuNP surface can induce significant conformational changes. Because of the interplay of these many effects, the configuration of the origami–AuNP complexes can be strongly influenced by the size, number, and surface functionalization of the attached NPs. These factors should therefore be taken into account when designing, assembling, and purifying constructs.

3. Conclusions

We have demonstrated low-acceleration rate-zonal centrifugation to be a facile, high-yield separation method for various complex AuNP–DNA origami constructs, enabling >90% purities to be reached. This method is scalable and non-destructive, and capable of high resolution.

It should be possible to further improve the separation resolution and the range of applicable particle sizes first by using nanoparticles with narrower size distributions[26] (Fig. S19†) and then, as diffusion becomes the dominant cause of band broadening, by minimizing its effect through the combined use of high-viscosity media to reduce diffusion coefficients and higher spin-speeds to shorten separation times. The technique can be further enhanced as an effective purification method of NP–DNA nano-hybrid structures by incorporating a nanoparticle "handle", which can only attach to well-folded structures, as the final part of an assembly, to permit separation of the target product. The ability to choose the mass of the "handle" enables the separation to be optimized. More design parameters are available: it is possible to distribute the desired mass in the form of multiple particles, and to choose their size and location to affect the conformation, and thus hydrodynamic radii of the constructs, to a greater or lesser extent. In addition, AuNPs enable direct visual detection of the target construct, greatly simplifying experimental extraction of the desired product. We expect that the high yields and purities obtained with this separation approach will open up the possibility of developing efficient, multi-step sequential reaction schemes for making more complex, hierarchical structures.

Finally, we have shown, through the comparison of hydrodynamic measurements and simulations of NP–origami constructs, that these systems exhibit complex conformational changes, caused by particle size-dependent interactions with ssDNA and dsDNA. By understanding the origins of these conformational changes, we can begin to devise ways of manipulating the particle–DNA interactions, *e.g. via* pH or salt concentration, to add additional, dynamic functionality to these constructs.

Acknowledgements

Dr S. H. Ko acknowledges support under the Cooperative Research Agreement between the University of Maryland and the National Institute of Standards and Technology Center for Nanoscale Science and Technology, Award 70NANB10H193, through the University of Maryland. Dr P. N. Patrone was supported by the National Institute of Standards and Technology American Recovery and Reinvestment Act Measurement Science and Engineering Fellowship Program Award no. 70NANB10H026 through the University of Maryland, with ancillary support from the NSF MRSEC under Grant no. DMR

05-20471, as well as the Condensed Matter Theory Center. Dr P. N. Patrone's research was also supported by NSF DMS0847587 at the University of Maryland. The authors are grateful to Dr V. A. Hackley and T. J. Cho for allowing us to use the DLS and helpful discussions. The authors thank Dr J. Schumacher for help with SEM imaging and also thank Dr J. Fagan for help with viscosity and density measurements. The authors also thank Dr V. Szalai for many helpful discussions.

Notes and references

1 N. R. Kallenbach, R. I. Ma and N. C. Seeman, *Nature*, 1983, **305**, 829.
2 P. W. K. Rothemund, *Nature*, 2006, **440**, 297.
3 B. Wei, M. Dai and P. Yin, *Nature*, 2012, **485**, 623.
4 Y. Ke, L. L. Ong, W. M. Shih and P. Yin, *Science*, 2012, **338**, 1177.
5 D. Han, S. Pal, Y. Yang, S. Jiang, J. Nangreave, Y. Liu and H. Yan, *Science*, 2013, **339**, 1412.
6 A. Kuzuya and M. Komiyama, *Nanoscale*, 2010, **2**, 309.
7 A. V. Pinheiro, D. Han, W. M. Shih and H. Yan, *Nat. Nanotechnol.*, 2011, **6**, 763.
8 V. Linko and H. Dietz, *Curr. Opin. Biotechnol.*, 2013, **24**, 1.
9 R. Carlson, *Nat. Biotechnol*, 2009, **27**, 1091.
10 J. J. Sobczak, T. G. Martin, T. Gerling and H. Dietz, *Science*, 2012, **338**, 1458.
11 D. Smith, V. Schüller, C. Engst, J. Rädler and T. Liedl, *Nanomedicine*, 2013, **8**, 105.
12 G. Bellot, M. A. McClintock, C. Lin and W. M. Shih, *Nat. Methods*, 2011, **8**, 192.
13 B. Ding, Z. Deng, H. Yan, S. Cabrini, R. N. Zuckermann and J. Bokor, *J. Am. Chem. Soc.*, 2010, **132**, 3248.
14 X. Shen, A. Asenjo-Garcia, Q. Liu, Q. Jiang, F. J. G. Abajo, N. Liu and B. Ding, *Nano Lett.*, 2013, **13**, 2128.
15 W. Mächtle and L. Börger, in *Analytical Ultracentrifugation of Polymers and Nanoparticles*, Springer-Verlag, Berlin, 2006.
16 J. Lebowitz, M. S. Lewis and P. Schuck, *Protein Sci.*, 2002, **11**, 2067.
17 G. Cadisch, M. Espana, R. Causey, M. Richter, E. Shaw, J. A. W. Morgan, C. Rahn and G. D. Bending, *Rapid Commun. Mass Spectrom.*, 2005, **19**, 1424.
18 C. Lin, S. D. Perrault, M. Kwak, F. Graf and W. M. Shih, *Nucleic Acids Res.*, 2012, **40**, 1.
19 L. Bai, X. Ma, J. Liu, X. Sun, D. Zhao and D. G. Evans, *J. Am. Chem. Soc.*, 2010, **132**, 2333.
20 X. Ma, Y. Kuang, L. Bai, Z. Chang, F. Wang, X. Sun and D. G. Evans, *ACS Nano*, 2011, **5**, 3242.
21 O. Akbulut, C. R. Mace, R. V. Martinez, A. A. Kumar, Z. Nie, M. R. Patton and G. M. Whitesides, *Nano Lett.*, 2012, **12**, 4060.
22 M. S. Arnold, A. A. Green, J. F. Hulvat, S. I. Stupp and M. C. Hersam, *Nat. Nanotechnol.*, 2006, **1**, 60.
23 J. A. Fagan, M. L. Becker, J. Chun and E. K. Hobbie, *Adv. Mater.*, 2008, **20**, 1609.
24 X. Sun, D. Luo, J. Liu and D. G. Evans, *ACS Nano*, 2010, **4**, 3381.
25 J. A. Fagan, M. Zheng, V. Rastogi, J. R. Simpson, C. Y. Khripin, C. A. Silvera Batista and A. R. Hight Walker, *ACS Nano*, 2013, **7**, 3373.
26 A. Fritsch, in *Preparative Density Gradient Centrifugations*, Beckman, Genève, 1975.
27 D. Velegol, S. Shori and C. E. Snyder, *Ind. Eng. Chem. Res.*, 2009, **48**, 2414.
28 T. Torring, N. V. Voigt, J. Nangreave, H. Yan and K. V. Kothelf, *Chem. Soc. Rev.*, 2011, **40**, 5636.
29 G. P. Acuna, F. M. Möller, P. Holzmeister, S. Beater, B. Lalkens and P. Tinnefeld, *Science*, 2012, **338**, 506.
30 A. Kuzyk, R. Schreiber, Z. Fan, G. Pardatscher, E. Roller, A. Hogele, F. C. Simmel, A. O. Govorov and T. Liedl, *Nature*, 2012, **483**, 311.
31 X. Shen, C. Song, J. Wang, D. Shi, Z. Wang, N. Liu and B. Ding, *J. Am. Chem. Soc.*, 2012, **134**, 146.
32 Z. Zhao, E. L. Jacovetty, Y. Liu and H. Yan, *Angew. Chem., Int. Ed*, 2011, **50**, 1.
33 B. Ding, Z. Deng, H. Yan, S. Cabrini, R. N. Zuckermann and J. Bokor, *J. Am. Chem. Soc.*, 2010, **132**, 3248.
34 Y. H. Roh, R. C. H. Ruiz, S. Peng, J. B. Lee and D. Luo, *Chem. Soc. Rev.*, 2011, **40**, 5730.
35 M. Endo, Y. Yang, T. Emura, K. HiDaka and H. Sugiyama, *Chem. Commun.*, 2011, **47**, 10743.
36 X. Shen, A. Asenjo-Garcia, Q. Liu, Q. Jiang, F. J. G. Abajo, N. Liu and B. Ding, *Nano Lett.*, 2013, **13**, 2128.
37 A. M. Hung, C. M. Micheel, L. D. Bozano, L. W. Osterbur, G. M. Wallraff and J. N. Cha, *Nat. Nanotechnol.*, 2010, **5**, 121–126.
38 D. Velegol, S. Shori and C. E. Snyder, *Ind. Eng. Chem. Res.*, 2009, **48**, 2414.
39 X. Pang, L. Zhao, W. Han, X. Xi and Z. Lin, *Nat. Nanotechnol.*, 2013, **8**, 426.
40 The width of the band due to diffusion and the initial band width is calculated by assuming diffusion occurs out of a slab of fixed initial concentration. The diffusion coefficient, D, can be calculated using the Stokes–Einstein relation; $D = kT/6\pi\eta R_H$, where k is Boltzmann's constant, T is the absolute temperature, η is the viscosity and R_H the hydrodynamic radius. The calculated nominal D of AuNP–DNA origami constructs is 3×10^{-12} m^2 s^{-1}, using $R_H =$ 35 nm and $\eta = 2$ mPa s as an initial value of the viscosity. To estimate a worst-case broadening, we assume a maximum centrifugation time of 270 min., and a band that is 0.5 mm thick upon loading. At the end of the centrifugation, this will have assumed a profile with a half-width at half-maximum of $\approx$ 0.4 mm. The standard deviation, σ, of the corresponding Gaussian distribution is $\approx$ 0.3 mm. This can be compared with typical band σ values of 1 mm. Assuming a root sum of squares addition, the effect of diffusion and the initial band width account for only about 5% of the observed broadening.
41 If we assume that pipetting can be used to extract all the material within $\pm\sigma$ of the band maximum, then a purity of 90% can be achieved as long as the maximum of next band (having the same spread) is at least 2.5σ away.

42 M. L. Mansfield, J. F. Douglas and E. J. Garboczi, *Phys. Rev. E: Stat., Nonlinear, Soft Matter Phys.*, 2001, **64**, 061401.
43 M. L. Mansfield, J. F. Douglas, S. Irfan and E. H. Kang, *Macromolecules*, 2007, **40**, 2575.
44 http://www.stevens.edu/zeno/.
45 J. F. Douglas, H. Zhou and J. B. Hubbard, *Phys. Rev. E: Stat., Nonlinear, Soft Matter Phys.*, 1994, **49**, 5319.
46 O. Padovan-Merhar, F. Vargas-Lara and F. Starr, *J. Chem. Phys.*, 2011, **134**, 244701.
47 S. Knauert, J. Douglas and F. Starr, *Macromolecules*, 2010, **43**, 3438.
48 K. Kremer and G. S. Grest, *J. Chem. Phys.*, 1990, **92**, 5057.
49 M. L. Mansfield and J. F. Douglas, *Macromolecules*, 2008, **41**, 5412.
50 S. Knauert, J. Douglas and F. Starr, *Macromolecules*, 2010, **43**, 3438.
51 L. M. Demers, C. A. Mirkin, R. C. Mucic, R. A. Reynolds, R. L. Letsinger, R. Elghanian and G. Viswanadham, *Anal. Chem.*, 2000, **72**, 5535.
52 H. D. Hill, J. E. Millstone, M. J. Banholzer and C. A. Mirkin, *ACS Nano*, 2009, **3**, 418.
53 S. J. Hurst, A. K. R. Lytton-Jean and C. A. Mirkin, *Anal. Chem.*, 2006, **78**, 8313.
54 J. Turkevich, *Gold Bull.*, 1985, **18**, 125.
55 J. J. Storhoff, R. Elghanian, C. A. Mirkin and R. L. Letsinger, *Langmuir*, 2002, **18**, 6666.
56 R. Schreiber, J. Do, E. Roller, T. Zhang, V. J. Schüller, P. C. Nickels, J. Feldmann and T. Liedl, *Nat. Nanotechnol.*, 2014, **9**, 74.
57 X. Zhang, T. Gouriye, K. Göeken, M. R. Servos, R. Gill and J. Liu, *J. Phys. Chem. C*, 2013, **117**, 15677.
58 J. Liu, *Phys. Chem. Chem. Phys.*, 2012, **14**, 10485.
59 P. Sandström and B. Åkerman, *Langmuir*, 2004, **20**, 4182.
60 H. Kimura-Suda, D. Y. Petrovykh, M. J. Tarlov and L. J. Whitman, *J. Am. Chem. Soc.*, 2003, **125**, 9014–9015; J. Turkevich, *Gold Bull.*, 1985, **18**, 125.
61 T. Herne and M. Tarlov, *J. Am. Chem. Soc.*, 1997, **119**, 8916.
62 L. Gearheart, H. Ploehn and C. Murphy, *J. Phys. Chem. B*, 2001, **105**, 12609.
63 M. Berg, R. Coleman and C. Murphy, *Phys. Chem. Chem. Phys.*, 2008, **10**, 1229.
64 S. Lacerda, M. Park, C. Meuse, D. Pristinski, M. Becker, A. Karim and J. F. Douglas, *ACS Nano*, 2010, **4**, 365.
65 J. Feng, R. Pandey, R. Berry, B. Farmer, R. Naik and H. Heinz, *Soft Matter*, 2011, **7**, 2113.
66 C. Goodman, N. Chari, G. Han, R. Hong, P. Gosh and V. Rotello, *Chem. Biol. Drug Des.*, 2006, **67**, 297.
67 B. Tinland, A. Pluen, J. Sturm and J. Weill, *Macromolecules*, 1997, **30**(19), 5763–5765.